


Maintenance mechanism of a circular surface wave in a magnetohydrodynamic cell and limits of its existence

Vladislav Eltishchev ^{*}, Gennadiy Losev [†] and Peter Frick [‡]

Institute of Continuous Media Mechanics UB RAS, Perm, Russian Federation



(Received 21 May 2024; accepted 23 July 2024; published 15 August 2024)

The circular surface wave (CSW) of a low-temperature gallium alloy in the immovable cell with a central bottom electrode and an upper ring electrode exposed to axial magnetic fields is studied experimentally. It is shown that, depending on the force parameter and geometrical characteristics of the cell [cell radius, height of the liquid metal (LM) layer, and position of the circular electrode], three modes can occur in the cell: rest, CSW, or axial rotation with a deep funnel on the surface providing the circular contact of the LM with the electrode. A mode map showing the boundaries of the CSW existence domain is plotted on the parameter plane. The mechanism which provides the existence of a stable CSW is suggested. It is shown that the CSW is a superposition of two intense large-scale vortices. The main vortex, whose axis coincides with the axis of the cylindrical cell, is generated by the Lorentz force localized near the bottom electrode and arising from the interaction of the divergent electric current with the vertical magnetic field. The intensity of the second vortex is an order of magnitude less, and the axis of rotation is directed to the contact area of the liquid metal with the ring electrode, which appears near the crest of the wave. Similar to the main vortex, it exists due to the interaction of the current converging to the contact area with the superimposed magnetic field. The second vortex provides the lifting of the LM ahead of the incoming wave. The intensity of both vortices is proportional to the product of the external field by the total current, which explains the linear relationship between the relative frequency of surface oscillations and their amplitude.

DOI: [10.1103/PhysRevFluids.9.083702](https://doi.org/10.1103/PhysRevFluids.9.083702)

I. INTRODUCTION

The stability of liquid metal (LM) surfaces attracted great interest in applied magnetohydrodynamics (MHD). The problem of instability of the liquid metal-electrolyte interface arose due to the development of large-scale aluminum electrolyzers [1–3]. The strong currents flowing in electrolyzers generate surface waves that can lead to short circuits. In the last decade, the stability of LM surface under strong electric current became a widely discussed problem in the context of creating the liquid metal batteries (LMB), which were developed as a promising candidate for large-scale electrical energy storage [4,5]. A basic LMB is a three-layer system which includes two layers of liquid metals of different densities and an electrolyte layer separating them. In both kinds of devices (electrolyzers and LMB), the passing of high electric current through the interface produces a strong surface wave, which can cause great damage in the multilayer system.

The wave that occurs in liquid metal as an inclined upper interface rotating about the axis of the cell is often called the metal pad roll (MPR) instability [6–8]. The MPR instability was first

*Contact author: eltishchev.v@icmm.ru

†Contact author: losev.g@icmm.ru

‡Contact author: frick@icmm.ru

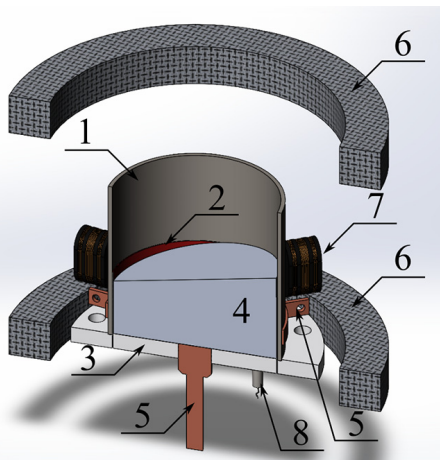


FIG. 1. Sketch of the experimental setup: 1 – stainless steel cylindrical cell, 2 – insulating coating, 3 – plexiglass bottom, 4 – liquid gallium alloy (with inclined surface), 5 – coaxial copper electrodes, 6 – Helmholtz coils, 7 – inductive level sensor (ILS), and 8 – UDV probe.

considered in the context of electrolyzers [9]. It was shown that this instability drives waves at the cryolite-aluminum interface inside Hall-Heroult cells. Similar instability is also possible in LMBs: during the charge/discharge process, strong electric currents flow through the three-layer liquid system, which can lead to MPR instability, i.e., to the appearance of gravity waves at the interfaces [7].

The MPR instability is caused by the fact that at the appearance of a wedge due to a large difference in conductivity between the electrolyte and the metal, a horizontal current component appears in the LM layer. This component interacts with the external magnetic field and gives rise to a pressure gradient directed across the line of surface inclination. The problem of MPR in a cylindrical cell has been analyzed in detail in [8].

Recently, it has been shown that such a circular surface wave (CSW) can be observed under the action of an external magnetic field in a cylindrical MHD cell, in which the current passes through an axial electrode on the cell bottom and a ring electrode on its side wall [10]. It was shown that, as the force parameter increases, the frequency of oscillation grows approximately according to the root law, and a further increase in the force leads to the degeneration of a circular surface wave into a rotating funnel. The CSW is not directly related to either electrolyzers or liquid-metal batteries, but both of these two applications define the interest in various liquid metal surface instabilities and prompt the study of surface MHD waves [11].

In this paper, we revisit the experimental study of CSWs in order to explain the mechanism of maintenance of a stable circular wave and to determine the limits of its existence in the governing parameter space.

II. EXPERIMENTAL SETUP AND METHODS

The experimental setup (Fig. 1) consists of a stainless steel cylindrical cell 1 with an inner radius of $R = 100$ mm and a height of 150 mm. The bottom 3 of the cell is made of plexiglass and is tightly connected to the side wall. The lower part of the inner surface 2 of the cell wall is insulated to a height of 80 mm. The cell is filled with gallium alloy $\text{Ga}_{86.3}\text{Zn}_{10.8}\text{Sn}_{2.9}$ (wt.%) 4 up to the fixed level below the insulation boundary [10].

The physical properties of the metal are as follows: density is 6256 kg/m^3 , coefficient of volume thermal expansion coefficient is $9.63 \cdot 10^{-5} \text{ 1/K}$, kinematic viscosity is $3 \cdot 10^{-7} \text{ m}^2/\text{s}$, conductivity

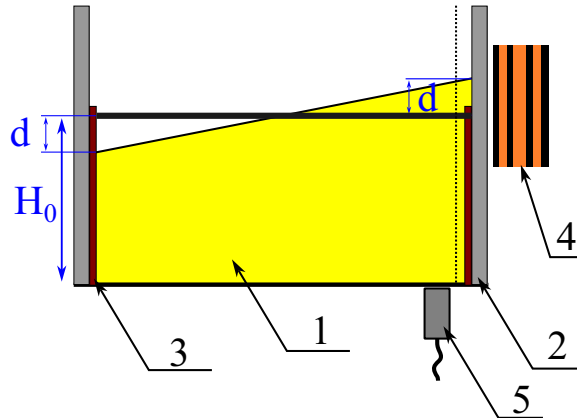


FIG. 2. Location of the level sensor on the experimental setup: 1. liquid metal, 2. conductive wall of the cell, 3. insulation layer, 4. ILS, and 5. UDV probe. Dashed line indicates the skin layer of metal.

is $3.56 \cdot 10^6$ Sm/m, sound speed is 2870 m/s, and melting point is $+17^\circ\text{C}$ [12]. The cell is continuously fed by argon to minimize the oxidation of the LM upper boundary.

The cylindrical copper cathode 5 of diameter $d = 30$ mm is located on the cell axis. The end face of the cathode is tinned and aligned with the bottom. The upper part of the side wall serves as the anode which is supplied through a copper tube, coaxially mounted outside the cathode. This coaxial supply compensates the magnetic field produced by supply cables to a large extent. The power supply provides a DC current from 400 to 800 A. A pair of Helmholtz coils 6 creates a constant vertical magnetic field in the range from 3.7 to 7.4 mT.

An ultrasonic Doppler velocimeter (UDV) probe (8) is installed in the plexiglass bottom at a distance of $r = 90$ mm from the center. Using the DOP 5000 device (Signal Processing, Switzerland), the profile of the vertical velocity component $v_z(z)$ and the echo signal reflected from the interface are measured.

In the experiments, the CSW was initiated by some mechanical perturbation on the LM surface. As a result a certain volume of fluid comes into contact with the uninsulated part of the side electrode. This causes an electric current to flow through the cell. The current interacts with the external magnetic field, which in turn generates an azimuthal component of the electromagnetic force. Under certain conditions, along with the rotation of the fluid within the layer, a steady azimuthal wave occurs, being in fact a CSW. For more details see [10].

The position of the LM upper boundary is recorded by eight inductive level sensors (ILS) 7 installed around the outside of the cell at the level of the upper boundary of the insulation. Each of the ILS consists of a set of three coils located coaxially [13].

Alternating current feeds the center coil, creating an alternating magnetic field, which in turn induces an electromotive force (EMF) in the measuring coils. If an electrically conductive medium occurs near one of the measuring coils, eddy currents are generated in it, decreasing the EMF in the corresponding measuring coil. The difference between the root-mean-square values of the EMF induced in two measuring coils determines the position of the LM surface near the cell wall.

The location of the level sensor on the experimental setup is illustrated in Fig. 2. Each sensor was precalibrated by determining the unperturbed horizontal metal level position. The sensor response is represented by a sigmoid curve, the central part of which corresponds to the metal level positions within the internal size of the sensor coils and is almost linear. The inner radius of the sensor coils was 40 mm, and the maximum recorded level deviations did not exceed 15 mm. The sensor coils were supplied with an alternating current of 500 Hz frequency, for which the skin layer thickness was about 12 mm. Thus, the sensor readings were determined by the values taken in the near-wall



FIG. 3. A sequence of photos of the liquid metal surface in CSW mode taken with a time step ~ 0.067 s (from left to right, from top to bottom). The insulator (colored in red) can be seen in the area of the surface level decrease.

region of the metal layer. The correction for the effect of surface slope was evaluated numerically for each point of the calibration curve [14].

III. RESULTS

The wave motion in the cell with liquid metal is illustrated in the sequence of photos shown in Fig. 3. The circular surface wave is clearly visible due to the part of the insulator protruding above the surface (bright red color). By analyzing its displacement, we can calculate the time required for the wave to complete a full revolution around the cell (in this example it is approximately 0.44 s). The fluid in the cell rotates intensively, as evidenced by the funnel near the axis of the cylinder.

Two examples of oscillograms recorded by the ILS are shown in Fig. 4. The first signal was recorded at a relatively weak forcing ($I = 400$ A, $B = 3.7$ mT), while the second signal was recorded at a current of $I = 600$ A and in the presence of a magnetic field of $B = 7.4$ mT. In both cases, the stable CSWs leading to quasiregular surface oscillations are observed. Note that the surface position near the sensor is counted from the level of unperturbed metal. The rotation of the metal leads to its displacement to the periphery, due to which the average value of the metal level at the wall significantly exceeds the value $d = 0$. The local signal maxima and minima are defined as d_{\max} and d_{\min} , respectively. The STD of local maxima and minima of ILS quasiharmonic signal are defined as δd_{\max} and δd_{\min} . It can be seen that, at weak rotation, the variations of local maxima and minima of the level are quite symmetric ($\delta d_{\max} \sim \delta d_{\min}$). At strong rotation, the local maxima of the level are significantly more stable than the local minima ($\delta d_{\max} \ll \delta d_{\min}$) (see Fig. 4).

The CSW is described by the magnitude

$$\Delta H = \frac{\langle d_{\max} \rangle - \langle d_{\min} \rangle}{2} \pm \frac{\delta d_{\max} + \delta d_{\min}}{2}. \quad (1)$$

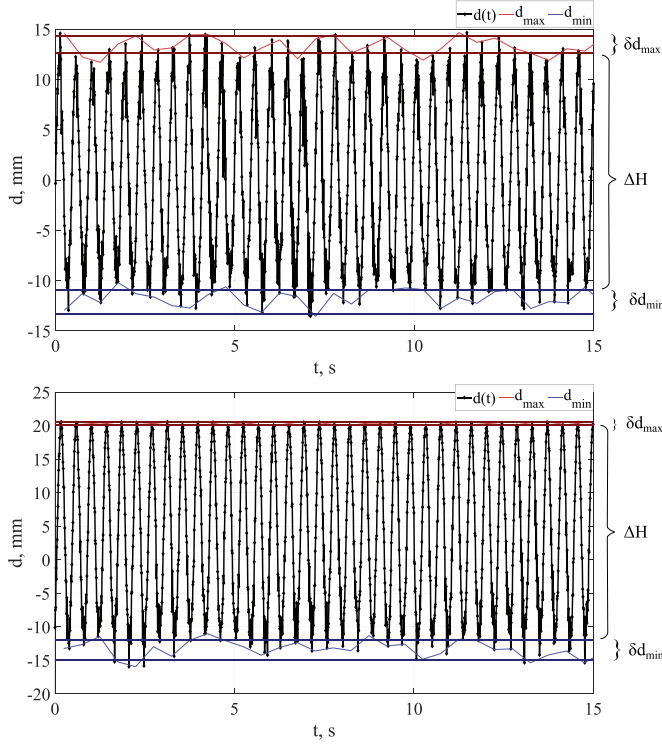


FIG. 4. ILS oscillograms for $I = 400$ A, $B = 3.7$ mT (top), and $I = 600$ A, $B = 7.4$ mT (bottom).

The latter term $(\delta d_{\max} + \delta d_{\min})/2$ determines the uncertainty of the ΔH measurement provided by the irregularity of oscillations of the free surface. Angle brackets indicate averaging over measurement time. Thus, the CSW is characterized by the amplitude ΔH and the frequency f .

In the absence of electromagnetic forces, any perturbation of the surface leads to a free decaying wave (running in a circle or standing), the frequency f_0 of which is determined by the gravity and fluid layer geometry [15]

$$f_0 = \frac{1}{2\pi} \sqrt{\frac{g\varepsilon_1}{R} \tanh\left(\frac{\varepsilon_1 H_0}{R}\right)}, \quad (2)$$

where R is the radius of the cell, g is the gravity acceleration, H_0 is the height of the fluid layer in undisturbed condition, and ε_1 is the first root of the derivative of the Bessel's function of the first kind. The frequency f_0 will be referred to below as the natural frequency of surface oscillations. For the actual parameters of the experimental setup, formula (2) gives $f_0 = 2.00 \pm 0.01$ Hz.

The electric current flowing through the liquid metal in a vertical magnetic field maintains a stable circular wave, and both characteristics of the CSW, i.e., the amplitude and frequency, are affected by the electromagnetic force parameters.

Taking the period of natural oscillations of the surface, $1/f_0$, as the unit of time and nondimensionalizing the Navier-Stokes equations, we obtain a dimensionless parameter S in front of the term, which describes the Lorentz force. This parameter governs the electromagnetic force effect on the LM layer and is determined by the electric current I flowing through the metal, the imposed external magnetic field B_0 , and the geometric parameters of the liquid metal layer [10],

$$S = \frac{I \cdot B_0}{\rho R^3 f_0^2}, \quad (3)$$

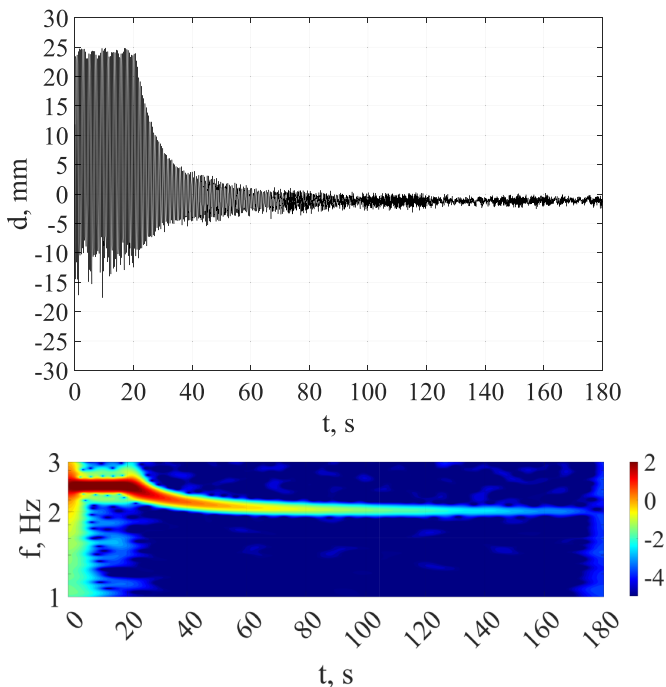


FIG. 5. A free decay of CSW: the ILS signal (top) and its wavelet spectrogram (bottom).

where ρ is the fluid density. In fact, the force parameter S is a version of the MHD interaction parameter widely used in magnetohydrodynamics [5–8,16]. It is basically the cross product of the current density and the magnetic field, defined using the characteristic spatial and temporal scales of the problem.

A. Amplitude-frequency response of CSW

Both the amplitude and frequency of CSW depend on the parameter S . Experimental results of CSW frequency measurements at different values of S were fitted by a root dependence $f \approx f_{\min} + a\sqrt{S}$, with $f_{\min} = 1.93$, which is about 3% below the estimation (2), and $a = 0.965$ [10].

There are two points that should be clarified before giving an explanation for the mechanism of circular waves. First, the determination of power γ in the form

$$f = f_0 + aS^\gamma \quad (4)$$

is complicated by the fact that the observed frequencies differ only slightly (within 25%) from the natural frequency, which requires a more accurate calculation of the frequency f_0 . Second, it is important to find out the law of change of the wave amplitude.

To refine the value of the natural oscillation frequency, we studied the decay of CSW after turning off the current source. Figure 5 presents an example of the ILS signal and its wavelet spectrogram, which includes 20 s before the current is turned off and about 160 seconds after. The CSW is characterized by a stable dominant frequency $f = 2.49$ Hz. When the current is turned off, the oscillations decay exponentially and the frequency shifts to lower values, asymptotically tending to the natural frequency of surface oscillations $f_0 = 2.02 \pm 0.01$ Hz. The wavelet analysis was done using the Morlet wavelet in the form $\psi = e^{2\pi it} e^{-t^2/2\sigma^2}$ with $\sigma = 4.5$, which provides good spectral resolution [17].

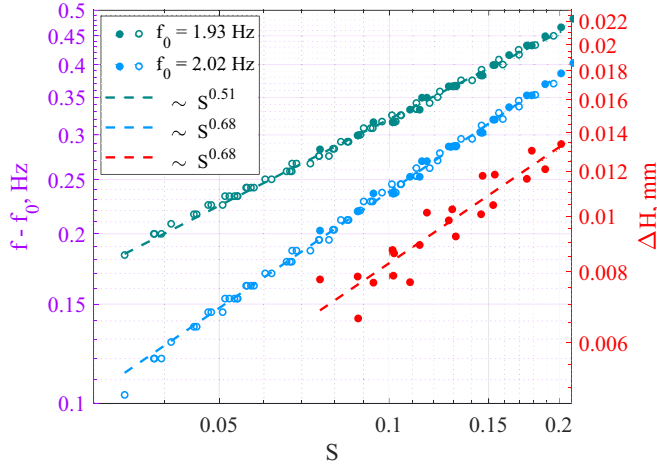


FIG. 6. The frequency shift $f - f_0$ and the wave amplitude ΔH versus the parameter S in log-log coordinates.

To check the power law (4), we plot in Fig. 6 the frequency shift $f - f_0$ versus the parameter S in double logarithmic coordinates. In fact, we show two fits: one for $f_0 = 1.93$ Hz, which gives $\gamma = 0.5 \pm 0.02$, and the other for $f_0 = 2.02$ Hz, which provides $\gamma = 0.68 \pm 0.02$. Note that in both cases we used the data from [10] (empty circles) and the new data from the current study (filled circles). It can be seen that the choice of the natural frequency strongly affects the power-law index. Taking into account the more accurate recent determination of this frequency, we accept the fit $f - f_0 \sim S^{0.68}$.

Figure 6 also shows the results of measuring the CSW amplitude at different values of the force parameter. The uncertainty in the estimates of the amplitude is significantly higher, but the power dependence with a slope close to the slope for the frequency is visible.

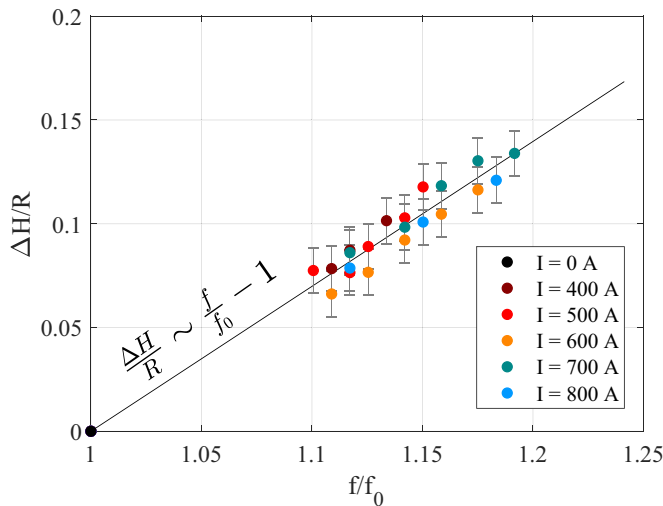


FIG. 7. CSW dimensionless amplitude-frequency response.

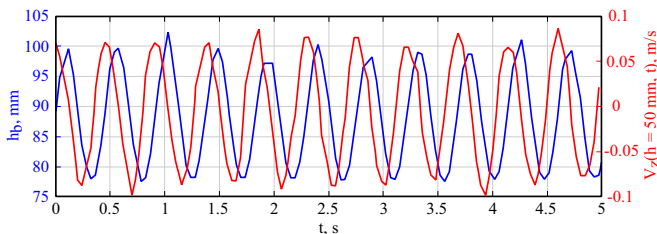


FIG. 8. Metal surface level (blue) and the vertical component of velocity (red) at $z = H_0/2$. Both signals are recorded by the UDV at $r = 0.9R$.

Figure 7 shows the dimensionless amplitudes of the wave $\Delta H/R$ versus the dimensionless frequency f/f_0 . As can be seen, the amplitude-frequency response is linear, which indicates a similar functional dependence of the CSW amplitude and frequency on the external force.

B. Maintenance mechanism of CSW in the MHD cell

Of primary importance for understanding the mechanism of maintenance of circular waves is the fact established above that there is a linear relationship between the amplitude and frequency (rotation velocity) of the circular wave generated by electromagnetic forces.

Another important point concerns the relationship between the surface wave and the structure of the velocity field in the cell. Direct measurements of the phase velocity of the wave and estimates of the rotational velocity of the liquid metal in the cell (obtained by analyzing the elevation of the average metal level at the periphery) showed that the values of these velocities are close. However, the rotation of the liquid metal can move the developed local surface elevation (depression), but it does not maintain it. The excessive local pressure and/or vertical movement of the fluid are required to support the local surface elevation. Figure 8 shows the liquid metal surface level and the vertical component of velocity at $z = H_0/2$ measured using an UDV. A steady phase shift between the two oscillatory processes is seen. The velocity fluctuations are ahead in phase of the surface fluctuations by 77° , i.e., a sufficiently intense upward fluid jet moves in a circle ahead of the wave hump. On the opposite side, the fluid naturally moves downward because there is a stable large-scale vortex in the cell, the axis of which is oriented predominantly horizontally and rotates relative to the axis of the cylindrical cell, lagging behind by about 13° from the diameter connecting the hump and trough of the wave. The maximum values of vertical velocity reach about 10% of the azimuthal velocity of the fluid.

The key point in explaining the mechanism of wave maintenance is the fact that the electric current flowing in the liquid metal is injected in the cell through two strictly localized areas: the central electrode at the cell bottom and the crest of the wave where there is an area of contact between the liquid metal and the ring electrode (see Fig. 9). The local supply of large currents to the liquid metal leads to the formation of so-called electrovortex flows (EVF) [18,19] generated due to interaction of the electric current with its own magnetic field. In the absence of external magnetic fields, EVF is a toroidal vortex in the center of which the velocity is directed from the electrode to the cell interior. Note that an axisymmetric vessel (cylinder, hemisphere) with a central electrode is a classical configuration for the EVF studies [16,20,21].

However, even sufficiently weak external magnetic fields can dramatically change the structure of the flow. The current flowing through the electrode and interacting with the magnetic field normal to the wall rotates the liquid metal. When the rotational flow energy reaches the EVF energy (even if it takes a sufficiently long time), a complete transformation of the flow structure takes place and the initial EVF is practically suppressed [22,23]. The transient regimes were studied experimentally and numerically in [24] and the mechanism of suppression of EVF and the structure of flows in

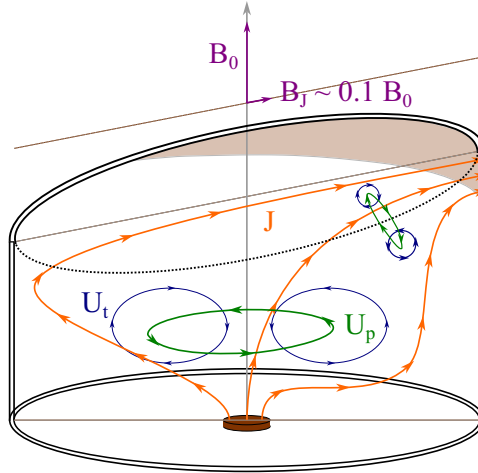


FIG. 9. Schematic representation of the CSW maintenance mechanism in the MHD cell.

magnetic fields of different intensities were comprehensively investigated in [23] to which we refer for details.

The magnetic field required for the CSW to arise significantly exceeds the threshold which ensures a transition from the toroidal EVF to the axial vortex. Therefore, the structure of the main large-scale flow (caused by the forces concentrated near the bottom electrode) exactly corresponds to that described in [23]. A strong azimuthal rotation develops in the cell against the background of which there exists a weak toroidal vortex with a downflow in the center (Fig. 9).

The formation of a vortex with a horizontal axis occurs in a similar way. The difference is that the symmetry is broken, since the contact region is a sickle-shaped strip, and only the projection of the external field B_0 on the direction of the current density vector near the contact region provides the vortex flow (assuming that the main electric current in the metal in the vicinity of the wall contact area is directed along the inclined surface [10]). Based on the estimation of the surface inclination near the wall, we obtain that the corresponding magnetic field component is within $B_J \lesssim 0.1B_0$. Thus, both vortices are due to the action of the Lorentz force, the total work of which is proportional to the product of the total current by the external magnetic field, which explains the linear relationship between the oscillation frequency (determined by the rotation velocity of the main vortex generated by the Lorentz force at the central electrode) and amplitude (determined by the velocity of the horizontal vortex generated by the Lorentz force near the contact with the wall at the crest of the wave). Since the wave crest is traveling in the upwelling direction, the observed phase shift between the velocity and surface oscillations is less than 90° .

C. Boundaries of the domain of CSW mode existence

The CSW mode exists within a limited range of governing parameters, which are the force parameter S and the relative difference between the undisturbed metal surface level and the sidewall insulation level $\delta H/R$.

At small height differences $\delta H/R$ and large S (fast rotation) the deformation of the LM surface leads to the contact along the entire perimeter and the formation of a funnel. On the contrary at large height differences $\delta H/R$ and small parameter S , the initial perturbation decays and the system returns to the equilibrium state. So, on the $(\delta H/R, S)$ parameter plane, there is a limited domain in which the CSW mode exists (Fig. 10).

The transition from the CSW mode to a funnel occurs due to a gradual increase of the average liquid metal level in the near-wall region. In the CSW mode there is always a small funnel near

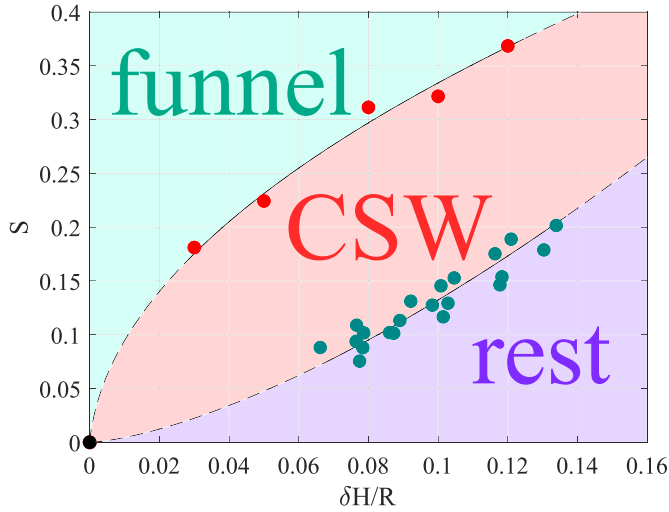


FIG. 10. Domain of existence of CSW mode, which is shown in the parameter space of power parameter S , and relative elevation of the electrode $\delta H/R$.

the cell axis caused by the rotation of the fluid. As the external force increases, the LM rotation velocity also increases and the funnel grows, which leads to raising the average level of metal in the near-wall region. leading to an increase in the average level of metal in the near-wall region. At the threshold value of S , the average fluid level in the near-wall region reaches the insulator boundary and the CSW maintenance mechanism disappears as the fluid rotates in constant contact with the side electrode.

The transition from steady waves to vortex when the parameter S reaches the threshold value S^* is illustrated by Fig. 11. In the experiment, for a given value of the $\delta H/R$ level, the S parameter was set to ensure the existence of stable waves. The S parameter was then sequentially increased by $\Delta S \approx 5 \cdot 10^{-3}$ with a waiting time after each increment of the order of 120 s. Figure 11 shows the ILS signal recorded during the transient process that began after the sequential increment of

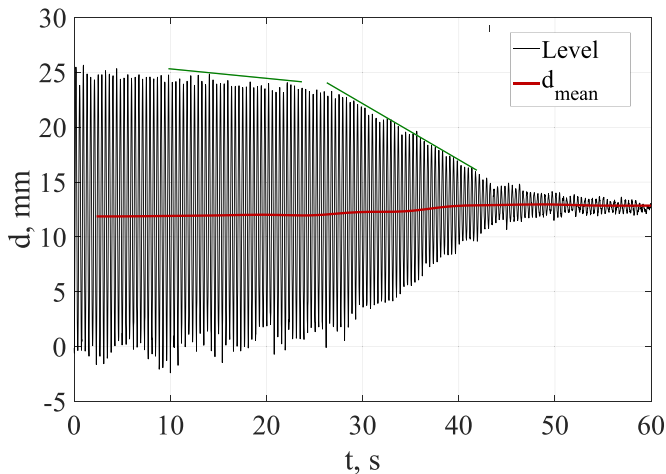


FIG. 11. Mode change when S reaches the threshold: the ILS signal (black line) and the average level of metal at the wall d_{mean} (red line).

the force parameter, corresponding on the graph to the time reference $t = 0$. The transient process develops gradually. A slow decrease in the amplitude begins at $t \approx 10$ s. At $t \approx 25$ s, the amplitude decreases by about 10% of the initial value. Within the next 15 s interval, a rather rapid decrease in the amplitude of oscillations occurs, which at $t \approx 40$ s is only $\sim 15\%$ of the initial value. It should be noted that the small fluctuations of the metal level at the wall are also observed after funnel formation, and the frequency of surface fluctuations even slightly increases (by about 2 – 3%).

The wave with an amplitude $\Delta H < \delta H$ decays due to the absence of contact between the liquid metal and the wall electrode and, consequently, due to the absence of the electromagnetic forcing. Thus, the lower limit of CSW existence can be determined from the curve showing the relationship between the oscillation amplitude and the force parameter.

The domain of existence of CSWs on the parameter plane $(\delta H/R, S)$ with experimentally recorded transition points is shown in Fig. 10. From above the domain of existence of CSW is bounded by the root line $S \sim \sqrt{\delta H/R}$, and from below by the power-law relation $S \sim (\delta H/R)^{1/\gamma} = (\delta H/R)^{1.47}$.

IV. SUMMARY

We proposed a mechanism for the support of a stable circular wave on the surface of liquid metal in an MHD cell. The cell has a central electrode at the bottom and a ring electrode covering the wall of the cylindrical cell above the metal level, and is in a vertical magnetic field. It is shown that the CSW is a superposition of two intense large-scale vortices. The main vortex, whose axis coincides with the axis of the cylindrical cell, is generated by the Lorentz force localized near the bottom electrode and arising from the interaction of the divergent electric current with the vertical magnetic field. The intensity of the second vortex is an order of magnitude less, and the axis of rotation is directed to the contact area of the liquid metal with the ring electrode, which appears near the crest of the wave. Similar to the main vortex, it occurs due to the interaction of the current converging to the contact area with the superimposed magnetic field, or, more precisely, with the projection of this field on the direction of the current density vector. This projection is an order of magnitude weaker than the vertical field, which determines the ratio of the intensities of the two vortices. The second vortex provides the lifting of the LM ahead of the incoming wave (the area of maximum vertical velocity of the metal rotates around the cell axis together with the whole metal, thus being ahead of the movement of the wave crest by 77°). The intensity of both vortices is proportional to the product of the external field by the total current, which explains the linear relationship between the frequency of surface oscillations and their amplitude.

Measurements of the natural frequency of oscillations of the LM surface in the cell were carried out. Based on the results obtained, the dependence of the CSW characteristics on the dimensionless force parameter S was determined. It is shown that both the frequency and amplitude of oscillations grow with increasing parameter according to the power law, $f/f_0 = 1 + aS^\gamma$, $\Delta H/R = bS^\gamma$ with the power index $\gamma = 0.68 \pm 0.02$.

Depending on the force parameter and geometrical characteristics of the cell (cell radius, height of the LM layer, and position of the circular electrode), three modes can be realized in the cell: rest, CSW, or axial rotation with a deep funnel on the surface providing circular contact of the LM with the electrode. A mode map showing the limit of the CSW existence is plotted on the parameter plane $(\delta H/R, S)$.

In concluding, we note that the wave motions of the considered type can arise not only in the vessels filled with liquid metal, where the electrodes are located above the metal level (this formulation of the problem in the context of technological applications may seem farfetched). In practice, similar waves can arise in an MHD cell in which the electrodes are the lower and upper ends of the cylinder if a gas bubble occurs in the cell. If, due to perturbations, the metal comes into contact with a part of the upper surface, a CSW similar to the one described in this paper will occur at appropriate control parameters.

ACKNOWLEDGMENTS

The work was carried out as part of a RMSE major scientific project (Agreement No. 075-15-2024-535, dated 23 April 2024).

- [1] I. M. Kirko, V. F. Al'Mukhametov, and S. Y. Khripchenko, Physical simulation of the unstable state of the electrolyte-metal interface in high-power aluminum electrolyzers, *Soviet Physics Doklady* **33**, 753 (1988).
- [2] V. Bojarevics, Interfacial MHD waves and associated heat distribution due to dynamic electric current interaction in an aluminium electrolysis cell, *Magnetohydrodynamics* **28**, 360 (1992).
- [3] P. A. Davidson and R. I. Lindsay, Stability of interfacial waves in aluminium reduction cells, *J. Fluid Mech.* **362**, 273 (1998).
- [4] H. Kim, D. A. Boysen, J. M. Newhouse, B. L. Spatocco, B. Chung, P. J. Burke, D. J. Bradwell, K. Jiang, A. A. Tomaszowska, K. Wang, W. Wei, L. A. Ortiz, S. A. Barriga, S. M. Poizeau, and D. R. Sadoway, Liquid metal batteries: Past, present, and future, *Chem. Rev.* **113**, 2075 (2013).
- [5] D. H. Kelley and T. Weier, Fluid mechanics of liquid metal batteries, *Appl. Mech. Rev.* **70**, 020801 (2018).
- [6] N. Weber, P. Beckstein, W. Herreman, G. M. Horstmann, C. Nore, F. Stefani, and T. Weier, Sloshing instability and electrolyte layer rupture in liquid metal batteries, *Phys. Fluids* **29**, 054101 (2017).
- [7] O. Zikanov, Shallow water modeling of rolling pad instability in liquid metal batteries, *Theor. Comput. Fluid Dyn.* **32**, 325 (2018).
- [8] W. Herreman, C. Nore, J. L. Guermond, L. Cappanera, N. Weber, and G. M. Horstmann, Perturbation theory for metal pad roll instability in cylindrical reduction cells, *J. Fluid Mech.* **878**, 598 (2019).
- [9] T. Sele, Instabilities of the metal surface in electrolytic alumina reduction cells, *Metall. Trans. B* **8**, 613 (1977).
- [10] V. Eltishchev, G. Losev, I. Kolesnichenko, and P. Frick, Circular surface wave in a cylindrical MHD cell, *Exp. Fluids* **63**, 127 (2022).
- [11] D. Munger and A. Vincent, A cylindrical model for rotational MHD instabilities in aluminum reduction cells, *Theor. Comput. Fluid Dyn.* **22**, 363 (2008).
- [12] A. Dobosz, Y. Plevachuk, V. Sklyarchuk, B. Sokoliuk, and T. Gancarz, Thermophysical properties of the liquid Ga–Sn–Zn eutectic alloy, *Fluid Phase Equilib.* **465**, 1 (2018).
- [13] V. Eltishchev, I. Dimov, A. Pavlinov, R. Khalilov, and I. Kolesnichenko, Inductive methods of detection the boundary of electrically conductive media in experiment, *IOP Conf. Ser.: Mater. Sci. Eng.* **581**, 012004 (2019).
- [14] V. Eltishchev, S. Mandrykin, and I. Kolesnichenko, Inductive level sensor: experiment and calculation, *IOP Conf. Ser.: Mater. Sci. Eng.* **950**, 012014 (2020).
- [15] M. Reclari, M. Dreyer, S. Tissot, D. Obreschkow, F. M. Wurm, and M. Farhat, Surface wave dynamics in orbital shaken cylindrical containers, *Phys. Fluids* **26**, 052104 (2014).
- [16] I. O. Teplyakov, D. A. Vinogradov, Y. P. Ivochkin, and I. B. Klementyeva, Experimental and numerical investigation of the instability of the electrovortex flow in hemispherical container, *Fluid Dyn. Res.* **50**, 051415 (2018).
- [17] P. G. Frick, D. D. Sokoloff, and R. A. Stepanov, Wavelets for the space-time structure analysis of physical fields, *Phys.-Usp.* **65**, 62 (2022).
- [18] V. Bojarevičs and E. V. Shcherbinin, Azimuthal rotation in the axisymmetric meridional flow due to an electric- current source, *J. Fluid Mech.* **126**, 413 (1983).
- [19] I. Kolesnichenko, S. Khripchenko, D. Buchenau, and G. Gerbeth, Electro-vortex flows in a square layer of liquid metal, *Magnetohydrodynamics* **41**, 39 (2005).
- [20] V. G. Zhilin, Y. P. Ivochkin, A. A. Oksman, G. R. Lurin'sh, A. I. Chaikovskii, A. Y. Chudnovskii, and E. V. Shcherbinin, An experimental investigation of the velocity field in an axisymmetric electrovortical flow in a cylindrical container, *Magnetohydrodynamics* **22**, 323 (1986).

- [21] W. Herreman, C. Nore, P. Ziebell Ramos, L. Cappanera, J. L. Guermond, and N. Weber, Numerical simulation of electrovortex flows in cylindrical fluid layers and liquid metal batteries, [Phys. Rev. Fluids](#) **4**, 113702 (2019).
- [22] P. Davidson, D. Kinner, R. Lingwood, D. Short, and X. He, The role of Ekman pumping and the dominance of swirl in confined flows driven by Lorentz forces, [Eur. J. Mech. B Fluids](#) **18**, 693 (1999).
- [23] P. Frick, S. Mandrykin, V. Eltishchev, and I. Kolesnichenko, Electro-vortex flows in a cylindrical cell under axial magnetic field, [J. Fluid Mech.](#) **949**, A20 (2022).
- [24] I. Kolesnichenko, P. Frick, V. Eltishchev, S. Mandrykin, and F. Stefani, Evolution of a strong electrovortex flow in a cylindrical cell, [Phys. Rev. Fluids](#) **5**, 123703 (2020).